

Long term behavior of the stirred vacuum on a Dirac chain: geometry blur and the random Slater ensemble

José Vinaixa,¹ Begoña Mula,¹ Alfredo Deaño,² Silvia N. Santalla,³ and Javier Rodríguez-Laguna¹

¹*Dto. Física Fundamental, Universidad Nacional de Educación a Distancia (UNED), Madrid, Spain*

²*Dto. Matemáticas, Universidad Carlos III de Madrid, Leganés, Spain*

³*Dto. Física & GISC, Universidad Carlos III de Madrid, Leganés, Spain*

(Dated: October 24, 2023)

We characterize the long-term state of the 1D Dirac vacuum stirred by an impenetrable object, modeled as the ground state of a finite free-fermionic chain dynamically perturbed by a moving classical obstacle which suppresses the local hopping amplitudes. We find two different regimes, depending on the velocity of the obstacle. For a slow motion, the effective Floquet Hamiltonian presents features which are typical of the Gaussian orthogonal ensemble, and the occupation of the Floquet modes becomes roughly homogeneous. Moreover, the long term entanglement entropy of a contiguous block follows a Gaussian analogue of Page's law, i.e. a volumetric behavior. Indeed, the statistical properties of the reduced density matrices correspond to those of a random Slater determinant, which can be described using the Jacobi ensemble from random matrix theory. On the other hand, if the obstacle moves fast enough, the effective Floquet Hamiltonian presents a Poissonian behavior. The nature of the transition is clarified by the entanglement links, which determine the effective geometry underlying the entanglement structure, showing that the one-dimensionality of the physical Hamiltonian dissolves into a random adjacency matrix as we slow down the obstacle motion.

I. INTRODUCTION

One of the most relevant insights obtained from quantum mechanics is the fact that a static *vacuum* is merely the ground state (GS) of a certain Hamiltonian. Therefore, its structure can be quite complex, and may present very relevant physical effects. For example, when a piece of vacuum is constrained by movable walls, they can feel Casimir forces [1]. If these walls move, they can induce transitions to excited states [2, 3]. Interestingly, the vacuum state typically presents quantum correlations, leading to entanglement between different regions. Moreover, the relation between the vacuum entanglement and geometry is known to run deeper than expected. For example, many low-energy quantum states respect the *area law*, i.e. the entanglement entropy (EE) between a region and its environment is proportional to the measure of its boundary [4, 5]. The area law has been rigorously proved in a few cases, such as the GS of gapped 1D Hamiltonians [6]. Yet, it receives logarithmic corrections in many critical states, as it is predicted by conformal field theory (CFT) [7, 8]. In fact, it is possible to read the underlying geometry of a quantum state without knowledge of the associated Hamiltonian, making use of the so-called *entanglement link* (EL) representation [9–11].

In this article we describe the long-term behavior of a portion of the 1D Dirac vacuum stirred by an impenetrable object moving through it. As a mental image, we may think of a piston moving through an empty cylinder, which would have no classical effect, but will have a considerable effect in quantum mechanics [12]. To that end, we define a toy model, which we call the *stirred Dirac vacuum*. In it, we start out with the GS of a free-fermionic chain, which can be used as a model of the Dirac vacuum in (1+1)D, and can be implemented phys-

ically using ultracold atoms in optical lattices [13–15]. We then introduce a classical obstacle, which acts like a movable boundary condition, canceling the local hopping amplitudes. This obstacle is forced to move forward, thus injecting energy into the system, and repeating its motion after reaching the end. In the long run, the instantaneous physical states will define a certain ensemble, which will depend on the velocity at which the obstacle moves. This dependence on the velocity of the quench has been highlighted in a variety of situations [16–19].

Since our system is subject to a periodic perturbation, we may describe it using a Floquet effective Hamiltonian [20–25], whose long term behavior may be described using random matrix theory (RMT) [26–29]. Moreover, random quantum states chosen according to a unitary-invariant measure are known to present *volumetric entanglement* and follow Page's law [30, 31]. Recently, the analogue for Gaussian states has been described [32–34], based on previous results from random matrix theory [35, 36], allowing us to characterize a *random Slater ensemble* (RSE). Yet, the approach of our stirred Dirac vacuum towards the RSE can be hindered by the existence of preserved quantities. As we will show, the values of the occupations of the Floquet modes within the initial state allow us to predict whether the RSE will be finally achieved or not, thus characterizing two different regimes, which can be further distinguished through their entanglement geometry via the aforementioned EL representation [9–11], showing that in the slow stirring phase the initial geometry is effectively blurred, while it remains if the stirring is fast.

This article is organized as follows. Sec. II describes our model and the simulation procedure. Then we describe our first numerical results in Sec. III, based on the energy absorption and the Floquet effective Hamiltonian,

finishing with an analysis of the Floquet occupations. In Sec. IV we provide the necessary background regarding the RSE, and we apply it to describe the long-term behavior of the slow phase in Sec. V. The transition between the slow and the fast phases is described in Sec. VI using the entanglement links. The article finishes summarizing our conclusions and proposals for further work.

II. THE STIRRED DIRAC VACUUM

Let us build a discrete analogue of the 1D Dirac vacuum on an N -site free-fermionic chain. In order to do that, we define *link* operators,

$$L_i \equiv -\frac{1}{2} \left(c_i^\dagger c_{i+1} + \text{h.c.} \right), \quad (1)$$

where c_i^\dagger and c_i are (spinless) fermionic creation and annihilation operators, with $i \in \{1 \dots N\}$, and the $1/2$ factor has been chosen for later convenience. Now, let us define our initial Hamiltonian, on a chain with open boundaries,

$$H_0 \equiv \sum_{i=1}^{N-1} L_i, \quad (2)$$

whose ground state (GS), containing $m = N/2$ particles, will constitute the initial state for our simulations, $|\Psi(0)\rangle$. Now, let us define a family of Hamiltonians,

$$H_i \equiv H_0 - L_{i+1}, \quad (3)$$

such that H_i has a broken link between sites $i + 1$ and $i + 2$, as it is depicted in Fig. 1 (a). Our system will be subject to Schrödinger's equation

$$i\partial_t |\Psi(t)\rangle = H(t) |\Psi(t)\rangle, \quad (4)$$

where

$$H(t) = H_i, \quad \text{if } t \in [(i-1)\tau, i\tau], \quad (5)$$

i.e.: $H(t)$ equals H_1 if $t \in [0, \tau]$, H_2 if $t \in [\tau, 2\tau]$, etc., up to time $T = (N-3)\tau$, check Fig. 1 (b). After that time, the full sequence repeats,

$$H(t+T) = H(t). \quad (6)$$

Therefore, at each instant t , one link of the chain will be absent, effectively splitting the initial chain into two disconnected parts, as if an impenetrable obstacle was interposed. The broken link will move along the chain, always rightwards, spending a fixed time τ on each position, and never leaving an isolated site at any time, and

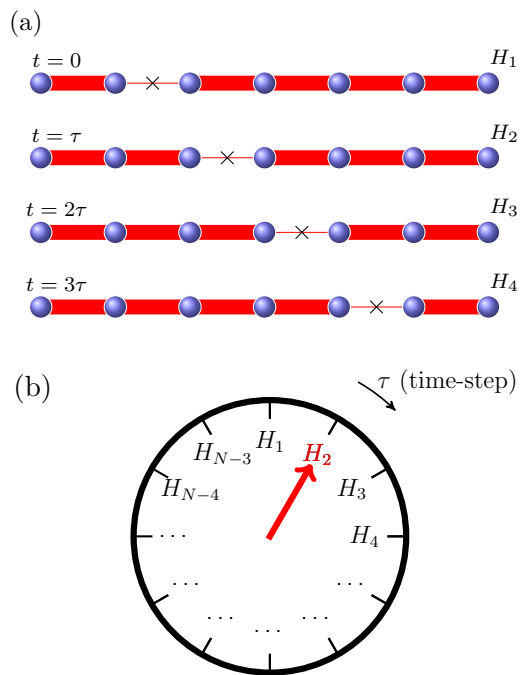


Figure 1. (a) Illustration of the discrete obstacle dynamics. A particular sequence of Hamiltonians $\{H_i\}$ is used to create a time-dependent $H(t)$, switching each H_i after a time-step τ . It may be described as an impenetrable obstacle moving along the chain. (b) This sequence may be represented as being driven by a stepper motor adjusted to a time delay τ , with total periodicity $T = (N-3)\tau$.

repeating its full pattern after time $T = (N-3)\tau$. Also notice that the obstacle moves in discrete steps, with an average velocity $v = 1/\tau$. Thus, the only relevant parameters of our model are the size N and the time-step τ . As we will see, *slow schedules* $\tau \gg 1$ and *fast schedules* $\tau \ll 1$ lead to a very different long-term behaviors of the system.

Let us stress that, in classical terms, the movement of the obstacle through the vacuum should bear no effect on its properties. Yet, the quantum nature of the state gives rise to an amplification of the vacuum fluctuations, and pairs particle-antiparticle will appear, in similarity to the dynamical Casimir effect [2, 3].

In the remainder of this section we will review some basic properties of the time-evolved quantum vacuum within our model.

The instantaneous Hamiltonian $H(t)$ can always be diagonalized in single-body terms. Therefore, the state $|\Psi(t)\rangle$ can always be written as a Gaussian state, or Slater determinant, which we can write as

$$|\Psi(t)\rangle = \prod_{k=1}^{N/2} b_k^\dagger(t) |0\rangle, \quad (7)$$

where $|0\rangle$ is the Fock vacuum, and the creation operators

$b_k^\dagger(t)$, which are usually called the occupied modes, can be written as

$$b_k^\dagger(t) = \sum_{i=1}^N U_{ki}(t) c_i^\dagger, \quad (8)$$

and $U_{ki}(t)$ are entries of an $N \times N$ unitary matrix, $U(t)$, which satisfies

$$i\partial_t U(t) = H(t)U(t). \quad (9)$$

The instantaneous correlation matrix is defined as

$$C_{ij}(t) \equiv \langle \Psi(t) | c_i^\dagger c_j | \Psi(t) \rangle = \sum_k \bar{U}_{ki}(t) U_{kj}(t), \quad (10)$$

and can be considered as a projector on the set of occupied modes, since it is hermitian and its spectrum is contained in $\{0, 1\}$. Moreover, let us stress that the single-body Hamiltonian, i.e. the matrix $h_{ij}(t)$ such that

$$H(t) = - \sum_{ij} h_{ij}(t) c_i^\dagger c_j, \quad (11)$$

is *bipartite*, i.e. there exists a bipartition of the set of sites (even vs. odd in our case) such that $h_{ij}(t)$ is nonzero only if i and j belong to opposite parts. This implies that the density in the GS,

$$\langle n_i \rangle = \langle c_i^\dagger c_i \rangle = 1/2, \quad (12)$$

for all times and that the instantaneous single-body energy spectrum, presents particle-hole symmetry [37], i.e., the eigenvalues of $h_{ij}(t)$ fulfill that

$$\varepsilon_k(t) = -\varepsilon_{N+1-k}(t). \quad (13)$$

Moreover, the information spread along the chain is limited by the Lieb-Robinson velocity, which corresponds to the Fermi velocity in our model, $v_F = 1$ [38].

Let us consider a block A composed of the left-most ℓ sites in the chain, $A = \{1, \dots, \ell\}$, when the state is a Slater determinant $|\Psi\rangle$, as in Eq. (7). Its entanglement properties are determined by the $N \times N$ correlation submatrix, C_A , defined by

$$(C_A)_{ij} = \sum_{k=1}^{N/2} \bar{U}_{ki} U_{kj}, \quad (14)$$

with $i, j \in A$ and zero otherwise. We realize that this matrix can be built as the product of three projectors,

$$C_A = P_A C P_A, \quad (15)$$

where P_A is the $N \times N$ matrix that projects on the ℓ sites of block A , and C is the full correlator matrix, which projects on the occupied modes. Let the spectrum of C_A be denoted by $\{\nu_k^A\}$, where each eigenvalue can be proved to lie in $[0, 1]$, as it corresponds to a truncated projector. It determines the entanglement entropy of block A , defined as

$$S_A \equiv -\text{Tr}(\rho_A \log \rho_A), \quad (16)$$

where $\rho_A = \text{Tr}_{\bar{A}} |\Psi\rangle \langle \Psi|$, through the following expression

$$S_A = \sum_{k=1}^m \text{H}_2(\nu_k^A), \quad (17)$$

where

$$\text{H}_2(x) \equiv -x \log(x) - (1-x) \log(1-x). \quad (18)$$

III. LONG TERM BEHAVIOR OF THE STIRRED DIRAC VACUUM

In this section we characterize the physical properties of the long-term stirred Dirac vacuum through numerical analysis of different observables: the absorbed energy, the mode occupations and the statistical properties of the Floquet spectrum.

A. Absorbed energy and vacuum friction

Let us consider the time-evolution of the total energy of the system, defined by the expectation value of the instantaneous Hamiltonian,

$$E(t) = \langle \Psi(t) | H(t) | \Psi(t) \rangle. \quad (19)$$

Notice that our system is isolated, and energy is pumped into it without any relaxation mechanism. Thus, we expect the total energy to grow, at least initially, which can be interpreted as a *vacuum friction*, provided by whatever forces make the obstacle move. Yet, as we will see, this energy growth must saturate at a certain moment, since our system is finite.

Fig. 2 shows the numerical results for the expected value of the energy $E(t)$ using $N = 256$ for several step-times τ , as a function of t/τ so that they reach the first cycle at the same point in the graph. The initial value can be estimated analytically, $E(0) \approx -N/\pi$ to a good approximation for large N [39]. Fig. 2 (a) shows the

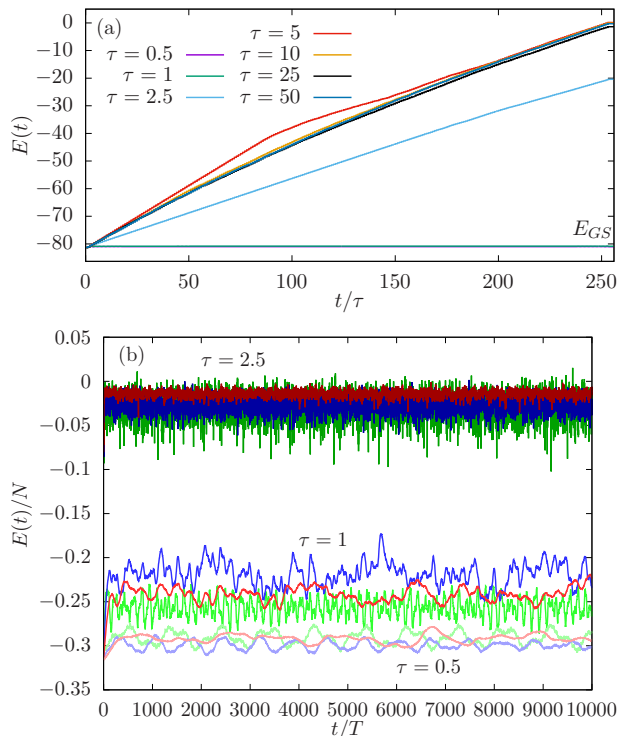


Figure 2. Expected value of total energy $\langle H(t) \rangle$, Eq. (19), as a function for time, for different values of the step-time τ . (a) Short-time behavior within the first period, $t < T$, for $N = 256$, as a function of t/τ . Notice that, for fast schedules, $\tau = 0.5$ and 1 , the energy absorption is extremely low in comparison with the slow ones. The bottom energy level corresponds to the initial GS value, E_{GS} . (b) Long-time behavior as a function of t/T , showing the expected value of the energy per site at the beginning of each cycle for $N = 64$ (green), 128 (blue) and 256 (red) and different color intensities for three values of $\tau = 0.5, 1$ and 2.5 , up to time $10^4 T$. Notice that in all cases the energy fluctuations seem to be stationary.

short-time absorption of energy, which is almost linear for short times. Interestingly, for large values of τ the curves coincide, while larger deviations can be found for intermediate values.

Fig. 2 (b) displays the energy per site $E(t)/N$ at the beginning of each cycle, for a much longer time-span, i.e. 10^4 full cycles, using three different sizes, $N = 64, 128$ and 256 , and three values of $\tau = 0.5, 1$ and 2.5 . The plots suggest that a stationary regime is reached for all the schedules, with an average value of the energy that grows with τ , saturating at $E \approx 0$. Moreover, both the amplitude and the time scales associated to the fluctuations depend both on N and τ . We may consider whether showing only the energies at the starting point of each cycle is creating a bias. Indeed, considering the full curve will add some fluctuations, but their amplitude is always small, and we have not considered them in the plots.

Thus, we are naturally led to consider the energy values as a stationary stochastic time-series for long enough

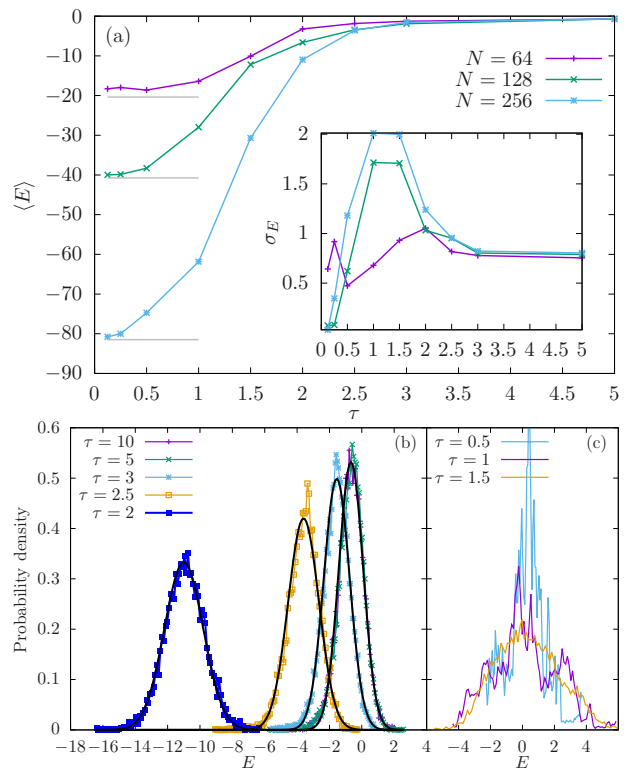


Figure 3. (a) Long-term expected value of the energy, $\langle E \rangle$, as a function of the step-time τ , for different system sizes, $N = 64, 128$ and 256 . The gray horizontal lines denote the initial values of the energy. The inset shows the standard deviation within the stationary regime. (b) Energy histograms for slow schedules, using always $N = 256$, $\tau \geq 2$ (left) and fast schedules, $\tau \leq 1$ (right, shifted to have zero average), showing a Gaussian fit whenever suitable.

times. Fig. 3 shows the statistical properties of the expected value of the energy. Panel 3 (a) shows the average value of the energy within the stationary regime as a function of τ for different system sizes N . We notice that, as τ grows, the expected value of the energy approaches zero, while for $\tau \rightarrow 0$ the expected value approaches $-N/\pi$, which is the initial energy of the system within a good approximation. The inset of Fig. 3 (a) show the standard deviation of the values of the energy within the stationary regime, showing a maximum at intermediate values of $\tau \approx 1$.

It is worthy to examine the full histogram of the values taken by the energy within the stationary regime, as they are shown in Fig. 3 (b). The left panel shows the histograms for $\tau \geq 2$, i.e. the slow schedules, along with suitable Gaussian fits. On the right panel we can see, superimposed, the converged histograms for $\tau = 0.5, 1$ and 1.5 , shifted so that their average becomes zero, which deviate substantially from the Gaussian distribution as τ decreases.

All these results lead us to conjecture that obstacle speeds larger than the Lieb-Robinson velocity, i.e. $\tau < 1$, lead to a fast regime which differs substantially from

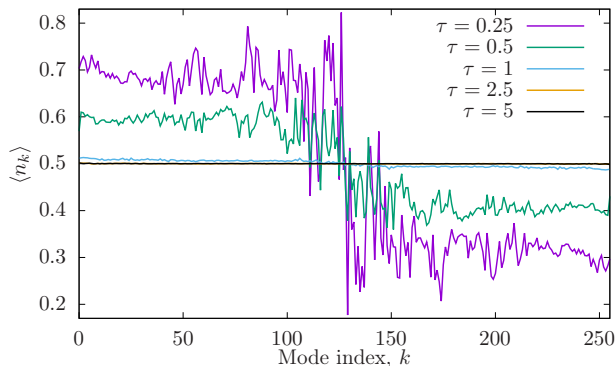


Figure 4. Long-term average occupation of the original Hamiltonian modes in the stationary regime, for different values of τ , using always $N = 256$.

the slow regime, characterized by $\tau \gg 1$, in which (a) the expected value of the energy approaches zero, (b) the energy fluctuations are Gaussian. Issue (a) can be readily explained, considering that the system becomes effectively thermalized at infinite temperature. Since the system respects particle-hole symmetry for all times, the expected value of the energy in this regime is zero, leading also naturally to Gaussian fluctuations of the energy. On the other hand, non-equilibrium quantum evolutions led by quantum coherences present typically non-Gaussian fluctuations in the energy [40–44].

B. Structure in momentum space

Let us consider $n_k = b_k^\dagger b_k$, i.e. the occupation operator associated to the k -th mode of the clean Hamiltonian H_0 , i.e.

$$b_k^\dagger = \sqrt{\frac{2}{N+1}} \sum_{i=1}^N \sin\left(\frac{\pi i}{N+1}\right) c_i^\dagger, \quad (20)$$

such that $H_0 = \sum_k \varepsilon_k n_k$, and $\varepsilon_k = -2 \cos(\pi k/(N+1))$. Initially, $\langle n_k(0) \rangle \equiv \langle \Psi(0) | n_k | \Psi(0) \rangle = 1$ if $\varepsilon_k < 0$, and 0 otherwise. In other words, the mode occupations follow a step function, $\langle n_k \rangle = \theta(N/2 - k)$.

We may wonder about the long-term evolution of $\langle n_k(t) \rangle$. Thus, we have obtained their time-averages within the stationary regime using $N = 256$ and different values of τ , as it is shown in Fig. 4. Indeed, we can see that in the slow regime, $\tau \gg 1$, the average occupations are flat, i.e. $\langle n_k \rangle \approx 1/2$ for all k , while within the fast regime, $\tau < 1$ we observe a complex pattern which, notwithstanding, remains more and more similar to the original step function as $\tau \rightarrow 0$.

C. Floquet effective Hamiltonian

The Hamiltonian imposed on our physical system is periodic, $H(t+T) = H(t)$, and therefore it is relevant to ask about the effective Floquet Hamiltonian, H_F , which is defined as the operator which would provide the same evolution after a single period, and can provide a lot of interesting information about the long-term behavior.

Let $U(t)$ be the evolution operator of our system, defined in terms of a time-ordered exponential [20, 25]. Then, we may define implicitly H_F through

$$U(T) \equiv \exp(-iH_F T). \quad (21)$$

The eigenvalues of H_F , $\{\epsilon_k\}$, are called *quasi-energies*, and are determined modulo $\Omega = 2\pi/T$. The properties of the Floquet Hamiltonian have been employed in order to characterize quantum chaotic behavior [27], associating Poisson level statistics to integrable systems and gaussian orthogonal or unitary ensemble (GOE/GUE) statistics to chaotic ones [21, 26, 29].

Fig. 5 (a) shows this scaled quasi-energy spectrum, $\epsilon_k \tau$ for different values of N and τ , showing an approximate collapse. Indeed, the quasi-energy spectrum is approximately linear throughout the range, presenting a slight curvature for $\tau \ll 1$. Thus, it is therefore relevant to ask about the level statistics. Fig. 5 (b) shows the cumulative distribution function (cdf) of the level separations, which are defined as

$$s_k \equiv \epsilon_{k+1} - \epsilon_k, \quad (22)$$

for $\tau = 0.5$ and 2.5 , using always $N = 256$, along with the Poisson distribution and the one associated to the gaussian orthogonal ensemble (GOE) for comparison, which are respectively given by

- Poisson, $p(s) = e^{-s}$.
- GOE, $p(s) = \frac{\pi}{2} s e^{-\frac{\pi}{4} s^2}$.

In order to characterize the crossover between the two regimes we have estimated the *double ratio* of the quasi-energies level distribution, defined as the average of the ratios [45, 46]

$$\tilde{r}_n \equiv \frac{\min(s_n, s_{n-1})}{\max(s_n, s_{n-1})} = \min(r_n, 1/r_n) \quad (23)$$

where $r_n = \frac{s_{n+1}}{s_n}$ are the ratios of consecutive level separations. The theoretical values for the average $\langle \tilde{r}_n \rangle$ for Poisson, GOE and GUE distributions are as follows,

$$\begin{aligned} \langle \tilde{r}_n \rangle_{\text{Poisson}} &\approx 0.38, \\ \langle \tilde{r}_n \rangle_{\text{GOE}} &\approx 0.54, \\ \langle \tilde{r}_n \rangle_{\text{GUE}} &\approx 0.59. \end{aligned} \quad (24)$$

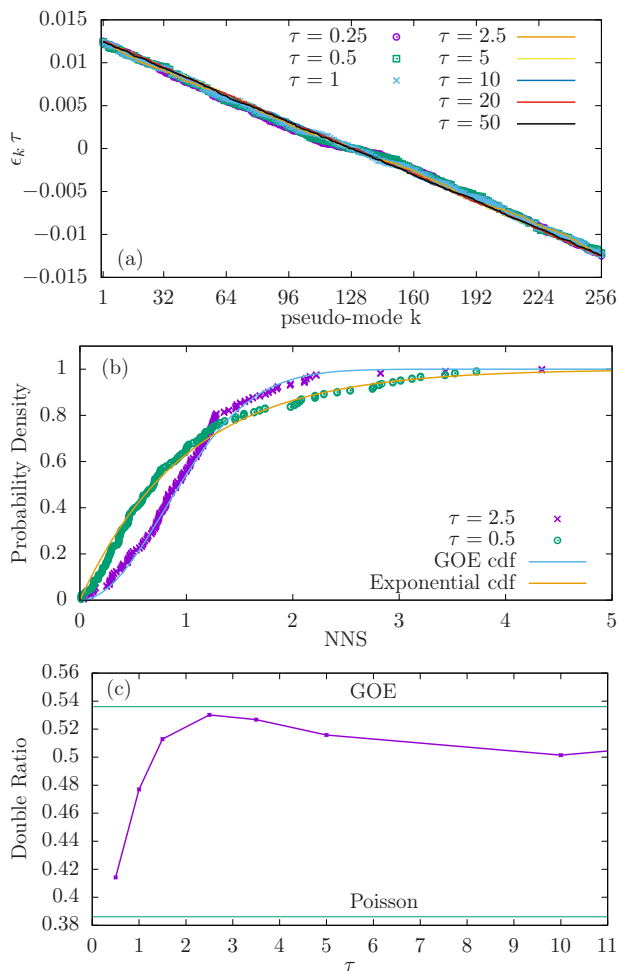


Figure 5. (a) Quasi-energy spectrum, $\tau \epsilon_k$ for different step-times τ , using system size $N = 256$ and time-steps ranging from $\tau = 0.25$ up to $\tau = 50$. The slow-driven regime is linear, with small non-linearities appearing around $\epsilon_k \approx 0$ for the fast-driven regime; (b) Cumulative distribution functions (CDF) of the level separations for $\tau = 0.5$ and 2.5 , along with the theoretically expected values corresponding to the Poisson and GOE distributions; (c) Double ratio of quasi-energy separations as a function of the step-time τ for $N = 256$, along with the theoretical values corresponding to the same distributions.

Fig. 5 (c) shows the double ratio $\langle \tilde{r}_n \rangle$ for our model driven at different speeds and using $N = 256$, displaying a crossover very similar to the one found in other situations more artificially constructed [46].

D. Floquet occupations

Conserved quantities are of extreme importance when describing any dynamical system. A time-independent free-fermion Hamiltonian always commutes with the number operators for a series of modes, thus providing us with N conserved quantities, i.e. the *occupations* for each mode. In our case, the Hamiltonian is time-dependent,

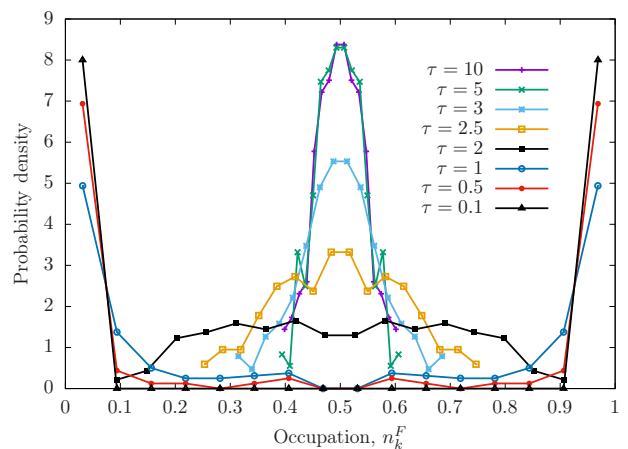


Figure 6. Histograms for the Floquet occupations, n_k^F , within the long-term evolution of a stirred Dirac chain with $N = 256$ and different values of τ . Notice a crossover between a fast regime, with a bimodal histogram concentrated on $n_k^F = 0$ and 1 , and a slow regime, with the values concentrated on $n_k^F = 1/2$.

but the time evolution can be mimicked using the Floquet effective Hamiltonian. We may thus define the Floquet occupations, $n_k^F \equiv \langle f_k^\dagger f_k \rangle$, where $H_F = \sum_k \epsilon_k f_k^\dagger f_k$ is the Floquet Hamiltonian. If we only observe the system at times $t_m = mT$, then these Floquet occupations are exactly preserved.

The values of the Floquet occupations, $\{n_k^F\}$, have been obtained for the initial state, $|\Psi(0)\rangle$, using $N = 256$ and several values for τ , and their histograms are shown in Fig. 6. Interestingly, their behavior is very different for slow and for fast schedules. When $\tau \ll 1$, the histogram becomes bimodal, essentially concentrated near $n_k^F = 0$ and 1 . On the other hand, for very slow schedules, $\tau \gg 1$, the histogram is concentrated around $n_k^F = 1/2$, reaching a finite value for the deviation in the large τ limit.

IV. THE RANDOM SLATER ENSEMBLE

Along the next sections we will argue that the stationary state for the slow schedule, $\tau \gg 1$, can be described as a statistical ensemble. Therefore, in this section we will present some basic facts about random fermionic Gaussian states.

Choosing a suitable unitary-invariant measure, we can pick up a random state in a Hilbert space of N qubits and find the expected value of its entanglement entropy when we separate a block of ℓ qubits. The results is known as Page's law [30],

$$\langle S(\ell) \rangle \approx \ell \log 2 - \frac{1}{2^{N-2\ell+1}}. \quad (25)$$

If our state is a Slater determinant, then Eq. (25) does not apply. Different researchers have considered this ex-

tension to the Page problem [33, 34], and we will provide in this section a simple explanation of the main results.

A Slater determinant is fully characterized by its correlation matrix, $C_{ij} = \langle c_i^\dagger c_j \rangle$, which can be regarded as a projector on a subspace of dimension m , the number of particles. Concretely, its reduced density matrix associated to a block A of size ℓ can be obtained by considering the associated submatrix, as it was expressed in Eq. (15), $C_A = P_A C P_A$, where P_A is the projector on the sites which belong to A . The spectrum of C_A , denoted by $\{\nu_k^A\}$, determines the entanglement spectrum and the entanglement entropy of block A in that state.

Let us consider the ensemble of Slater determinants on N sites with m fermionic particles, which are chosen according to the Haar measure in $U(N)$, i.e. we choose a random unitary matrix V from the gaussian unitary ensemble (GUE), truncate its first m columns, and form the correlation matrix $C = VV^\dagger$. Alternatively, we may write an $N \times m$ matrix with Gaussian entries (with zero mean and unit variance both for the real and imaginary parts), and let it undergo a Gram-Schmidt procedure. Any such submatrix C_A , of dimension $\ell \times \ell$, is said to belong to the *Jacobi ensemble* [36]. If we let $m = N/2$ and define $\mu = \ell/N$, assuming that $\mu \leq 1/2$, we can obtain an expression for the eigenvalue density, which simplifies slightly if we define $\lambda_k^A \equiv 2\nu_k^A - 1$. Indeed,

$$\rho_\mu(\lambda) = \frac{\sqrt{4\mu(1-\mu) - \lambda^2}}{2\pi\mu(1-\lambda^2)}, \quad (26)$$

which is only defined in the interval between $\lambda_\pm(\mu) \equiv \pm 2\sqrt{\mu(1-\mu)}$. If the eigenvalues were uncorrelated, the average entanglement entropy would be written as

$$\langle S_A \rangle \approx \mu N \langle H_2(\mu) \rangle. \quad (27)$$

with

$$\langle H_2(\mu) \rangle = \int_{\lambda_-(\mu)}^{\lambda_+(\mu)} H_2\left(\frac{\lambda+1}{2}\right) \rho_\mu(\lambda) d\lambda. \quad (28)$$

Appendix A proves that

$$\langle H_2(\mu) \rangle = \log(2) - 1 - \frac{(1-\mu)}{\mu} \log(1-\mu), \quad (29)$$

thus leading to

$$S(\ell) \approx \ell \log(2) - \ell - (N - \ell) \log\left(1 - \frac{\ell}{N}\right). \quad (30)$$

For the half-chain, $\ell = N/2$, we have

$$S(N/2) \approx N \left(\log(2) - \frac{1}{2} \right), \quad (31)$$

which is lower than the Page law equivalent. Indeed, the entropy per site appears to be $2\log(2) - 1 \approx 0.386$ in the random Slater ensemble while it is $\log(2) \approx 0.693$ in the Page ensemble.

The results presented above are only approximate, because the eigenvalues from a single matrix can not be considered to be uncorrelated. The exact statistical properties for the entropy were obtained in [33, 34] and present a small correction with respect to our simple approximation. In our notation,

$$\begin{aligned} \langle S(\ell) \rangle &= 1 - \mu(1+N) - m\mu\Psi(m) + N\Psi(N) \\ &\quad + \mu(m-N)\Psi(N-m) + (\ell-N)\Psi(N-\ell+1) \end{aligned} \quad (32)$$

for $\ell \leq N/2$, where $\Psi(x) = \Gamma'(x)/\Gamma(x)$ is the digamma function. Its variance, in turn, can be expressed as

$$\begin{aligned} (\Delta S_A)^2 &= \log(1-\mu) + \mu + \mu^2 \\ &\quad + \mu^2 \left(2\frac{m}{N} - 1 \right) \log\left(\frac{N}{m} - 1\right) \\ &\quad + \mu(\mu-1) \left(\frac{m}{N} - 1 \right) \frac{m}{N} \log^2\left(\frac{N}{m} - 1\right) + O(1), \end{aligned} \quad (33)$$

which reduces to $(\Delta S_A)^2 = \log(1-\mu) + \mu + \mu^2$ in the case of half-filling.

We have performed numerical experiments with random unitary matrices in order to check the validity of Eqs. (26), (30) and (32), and the results are shown in Fig. 7. Panel (a) shows the eigenvalue histogram of 500 matrices sampled from systems with $N = 256$ and different values of ℓ . Panel (b) shows the expected value of the entanglement entropy from our numerical experiments, comparing to our approximation, Eq. (30), and the exact theoretical prediction, Eq. (32). We may conclude that our simple approximation is quite accurate.

V. ENTANGLEMENT IN THE STIRRED DIRAC VACUUM

Let us now discuss the statistical properties of the entanglement structure in the long-term stationary state of the stirred Dirac vacuum considered in Sec. III. As we will show, the slow and the fast schedules present very different behaviors, and the slow phase corresponds to the random Slater ensemble discussed in the previous section.

Fig. 8 (a) shows the time evolution of the EE associated to the partition defined by the position of the obstacle, as a function of time divided by τ (i.e. the position), for different values of τ , using always $N = 256$, and only for the first period, $t \leq T$. Notice that the initial growth

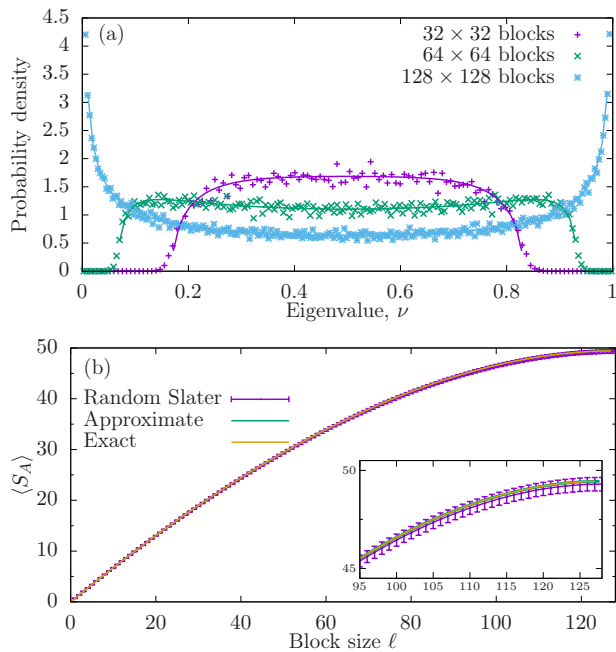


Figure 7. (a) Spectral density for random Slater truncated correlation matrices with $N = 256$ and different values of the block size ℓ , comparing with Eq. (26); (b) Expected value of the entanglement entropy obtained from the same data, along with the two approximate and exact theoretical curves, Eq. (30) and (32), with their errorbars. Inset: zoom up of the upper-right part of the panel, in order to highlight the small differences between the curves.

rate increases with the time-step. Yet, the maximum is reached at a time which decreases with τ , corresponding to the moment in which the information of the initial quench—which travels at the Lieb-Robinson velocity—reaches the opposite boundary, bounces back and meets the obstacle again. Simple kinematic arguments show that this time, t_B , fulfills

$$t_B = 2L \frac{\tau}{\tau + 1}, \quad (34)$$

which is signaled by the vertical marks in Fig. 8 (a). The second knee in the entropy curve for $\tau = 10$ corresponds to the second rebound, but further rebounds are no longer coherent enough to show up in the curve.

Alternatively, we can also consider the time evolution of the EE per site of a fixed partition, e.g. the left half, as it is shown in Fig. 8 (b), on a larger time scale, as a function of t/T . It can be observed that, in the long run, the entropy also reaches a stationary regime, as we found for the energy, and also in this case the long-term average and deviation depends both on N and τ .

Following the analysis performed for the entropy, we plot in Fig. 9 (a) the long-term average of the half-chain entropy per site as a function of τ for $N = 64, 128$ and 256 . We again observe a crossover between a low entropy phase for fast schedules, $\tau < 1$ and a high entropy phase for slow schedules, $\tau \gg 1$. The theoretically expected

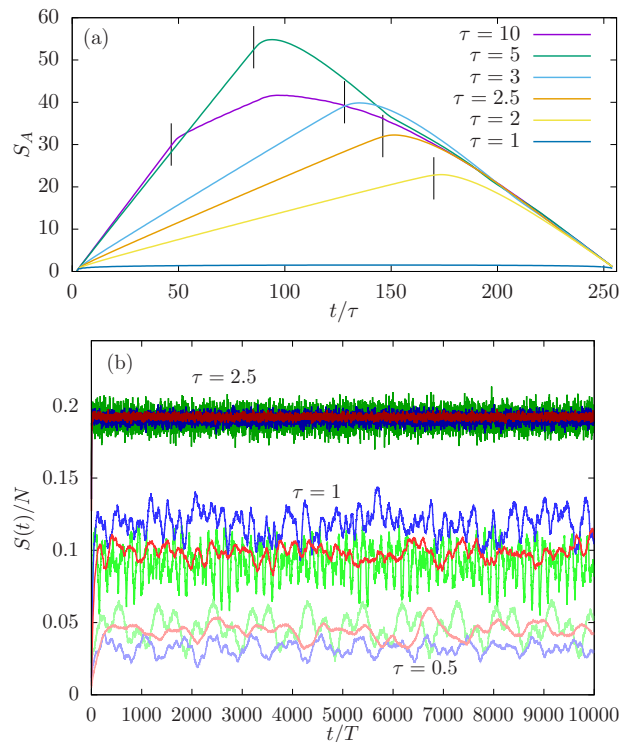


Figure 8. (a) EE of the partition associated to the obstacle for $N = 256$, and a range of values of the step-time τ . The vertical marks denote the expected time for the rebound of the quench information; (b) EE of the half chain as a function of time, within a larger time-span using $N = 64$ (green), 128 (blue) and 256 (red), and using color intensity to denote different values of $\tau = 0.5, 1$ and 2.5 .

value of the entropy per site, $\log(2) - 1/2$, is shown as a horizontal grey line.

Fig. 9 (b) shows the entropy histogram for $N = 256$ and larger values of τ on its left panel, $\tau = 2, 2.5, 3$ and 5 , along with a suitable Gaussian fit. On the right panel we observe the histogram of the entropy for lower values of the time-step τ , showing that they do not present a Gaussian shape.

Now, let us address our main question in this section: does the stationary regime of the stirred Dirac vacuum correspond to the Jacobi class? The best approach is to compare the predictions for the EE and for the eigenvalues of the truncated correlation matrices, as we do in Fig. 10. Indeed, in panel (a) we observe that the average values of the spectral density for the aforementioned correlation matrices follow the Jacobi law, Eq. (26), using $N = 256$, $\tau = 10$ and three block sizes. Moreover, the average values of the EE also follow the predictions of Eq. (30) and (32). In this case, we plot both theoretical curves along with the averages obtained for the random Slater ensemble and the stirred Dirac vacuum using again $N = 256$ and $\tau = 10$. The inset highlights the tiny differences which can be observed between them.

Let us also consider the average entropy profile in the

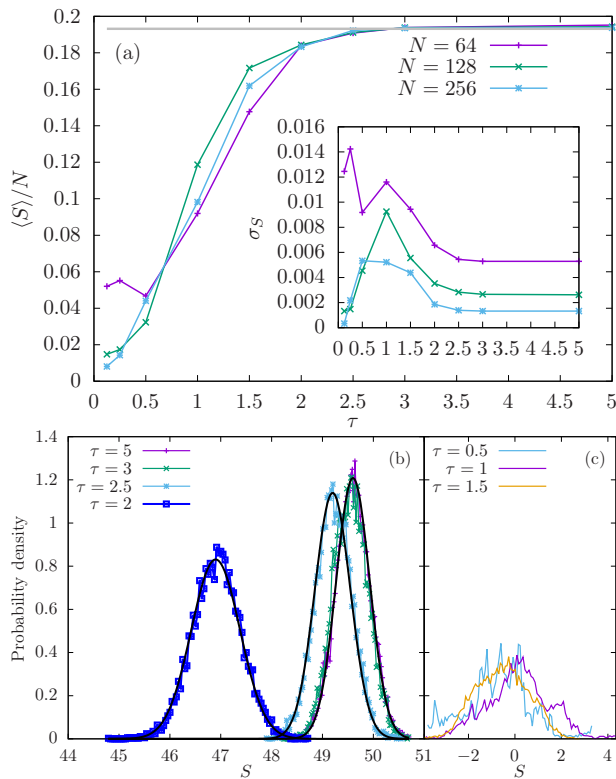


Figure 9. (a) Long-term expectation value of the half-chain entropy per site, $\langle S \rangle$, as a function of the step-time τ , for different system sizes, $N = 64, 128$ and 256 . The gray horizontal lines denote the theoretical prediction for the long-term entropy per site. The inset shows the standard deviation within the stationary regime. (b) Entropy histograms for slow schedules, using always $N = 256$, $\tau \geq 2$ (left) and fast schedules, $\tau \leq 1$ (right), showing a Gaussian fit whenever suitable.

stationary state for different values of τ , which is shown in Fig. 11, which plots the value of $\langle S(\ell) \rangle$ for $N = 256$. We can see that for $\tau = 2.5, 5$ and 10 the entropy fits the theoretical prediction (shown in black). For $\tau = 1$ and $\tau = 0.5$ the entropy is much lower, and we have fitted it to a different law [47],

$$S(\ell) \approx A + B \sin\left(\frac{\pi\ell}{N}\right) + C \sin\left(\frac{3\pi\ell}{N}\right). \quad (35)$$

Finally, we have considered the joint statistical properties of the entropy and the energy, and measured the correlation coefficient of the corresponding time series, defined as

$$\text{Corr}(E, S) \equiv \frac{\langle ES \rangle}{\sigma(E)\sigma(S)}. \quad (36)$$

The results are shown in Fig. 12, as a function of τ for different system sizes. We see that in all cases the correlation is close to one for fast schedules, and close to zero for $\tau \gg 1$, thus putting forward another feature of the

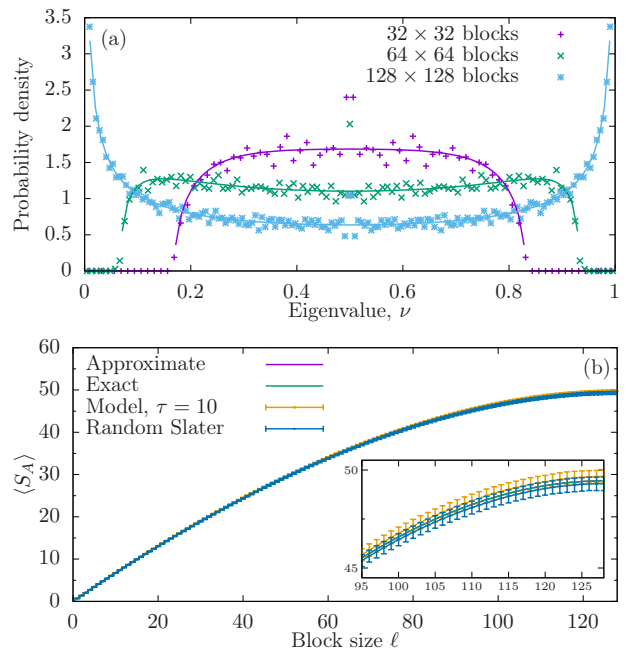


Figure 10. (a) Spectral density for the stirred Dirac vacuum for the truncated correlation matrices with $N = 256$ and different values of block size ℓ , comparing with Eq. (26), for a large step-time $\tau = 10$; (b) Expected value of the entanglement entropy obtained from the same data, along with the two approximate and exact theoretical curves, Eq. (30) and (32). The inset highlights the tiny difference between the theoretical calculations, and between those and the numerical results for the random Slater model and the stirred Dirac vacuum.

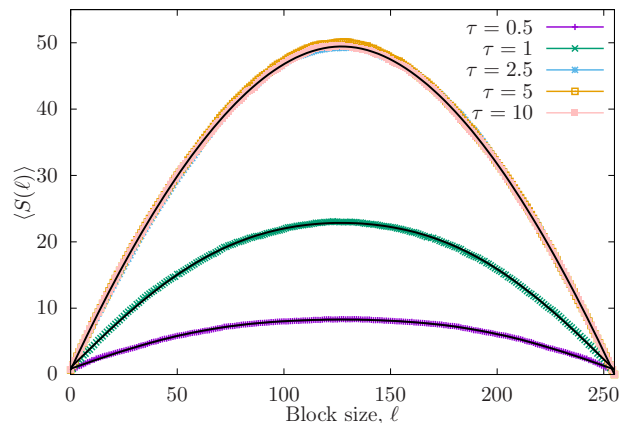


Figure 11. Long-term average of the entropy profiles for $N = 256$ and different values of τ , along with the theoretical expectations. For $\tau \gg 1$ we have shown Eq. (30) in black, while for lower values of τ we have fit to the form (35).

slow schedule phase, the independence of the fluctuations of S and E .

A relevant question is in order. Since the system possesses N exactly preserved quantities, i.e. the Floquet occupations shown in Sec. IIID, how is it possible that

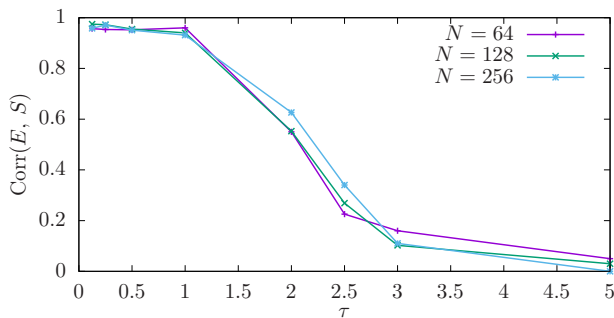


Figure 12. Correlation coefficient of entropy and energy for the random Slater model, as a function of τ for different values of N .

the long-term state of the stirred Dirac vacuum resembles the RSE for large τ ? The answer is that, in the slow regime, the values of the Floquet occupations *resemble* the expected values within the RSE, which is always $1/2$. Thus, we may conjecture that the actual ensemble explored in the long-term by the stirred Dirac vacuum can be described by a generalized RSE, in similarity to the generalized Gibbs ensemble, in which we force the expected values of a certain set of occupations to take values far from $1/2$.

VI. ENTANGLEMENT LINKS AND THE GEOMETRY BLURRING TRANSITION

The nature of the transition between the fast and slow schedules can be very clearly characterized using the *entanglement link* (EL) representation, which was recently introduced by some of us [9–11]. The key insight behind the EL is to take seriously the area law of entanglement, and to propose the existence of an adjacency matrix J_{ij} which approximately represents the entanglement entropy of every block A ,

$$S_A \approx \sum_{i \in A, j \in \bar{A}} J_{ij}. \quad (37)$$

The EL representation is only exact in a few cases, such as valence bond states [9], but it is surprisingly accurate in most situations, including typical ground states and time-dependent states after a quantum quench [11]. Even random states possess reasonably accurate EL representations [10]. The EL of the GS of a gapped chain can be proved to be exponentially concentrated along the main diagonal, while for a critical homogeneous chain the EL fall as a power law, $J_{ij} \sim |i-j|^{-2}$, still showing clear signals of the original geometry of the Hamiltonian. The EL can be numerically obtained for Slater determinants in a fast way [10]. Defining $S_{i,j}$ as the entanglement entropy of the block $\{i, i+1, \dots, j-1\}$ (with periodic boundaries), we obtain

$$J_{ij} = S_{i,j} - S_{i+1,j} - S_{i,j+1} + S_{i+1,j+1}. \quad (38)$$

In Fig. 13 we show the EL matrix for $t = 1275T$ using $N = 256$ and several values of τ . We can see that in the fast cases, i.e., $\tau = 0.005, 0.5$ and 1 , the EL matrix preserves the 1D structure that the state inherits from the original Hamiltonian. Yet, in the slow case the entanglement links appear to be homogeneously spread, thus showing that the original geometry has been effectively blurred.

The geometry blurring transition may be further characterized by the fraction of entanglement links along the different subdiagonals, i.e.

$$f_r \equiv \frac{\sum_{i=1}^{N-r} J_{i,i+r}}{\sum_{i,j} J_{i,j}}, \quad (39)$$

which should decay as r^{-2} for fast schedules, and remain constant ($\sim 1/N$) for slow ones. Fig. 14 shows that, indeed, the values of f_r become constant for large values of τ , except for the final lattice effects, hinting at the idea that the geometry has been blurred.

VII. CONCLUSIONS AND FURTHER WORK

We have considered the long-term behavior of the (1+1)D stirred Dirac vacuum, which is defined as a free-fermionic chain in its ground state, with an obstacle traveling through it, spending a time τ on each link. In classical terms, the motion of the obstacle would be completely free, but in quantum terms we observe a drag force which transfers energy to the state. After some time, a stationary regime is reached, which we have characterized using different tools. In all cases, we observe a different behavior in the *slow* and in the *fast* regimes, defined by comparing the obstacle velocity and the Lieb-Robinson velocity of the system.

In the slow regime, the average energy reaches the value zero, which corresponds to a thermal state at infinite temperature. Also, the Floquet effective Hamiltonian presents a GOE spectrum, which suggests a connection to quantum chaos. Furthermore, the state can be accurately represented by the *random Slater ensemble*, which has been recently described, in which the occupied orbitals are randomly chosen according to a Haar measure. The entanglement spectrum histogram and the average entanglement entropy can be predicted using random matrix theory, making use of the Jacobi ensemble. We have shown that, indeed, the entanglement entropy slow schedules corresponds to the random Slater prediction.

It is interesting to notice that, in all cases, the system possesses a large number of exactly conserved quantities, corresponding to the occupations of the Floquet modes. Yet, only in the slow regime, the expected values of these

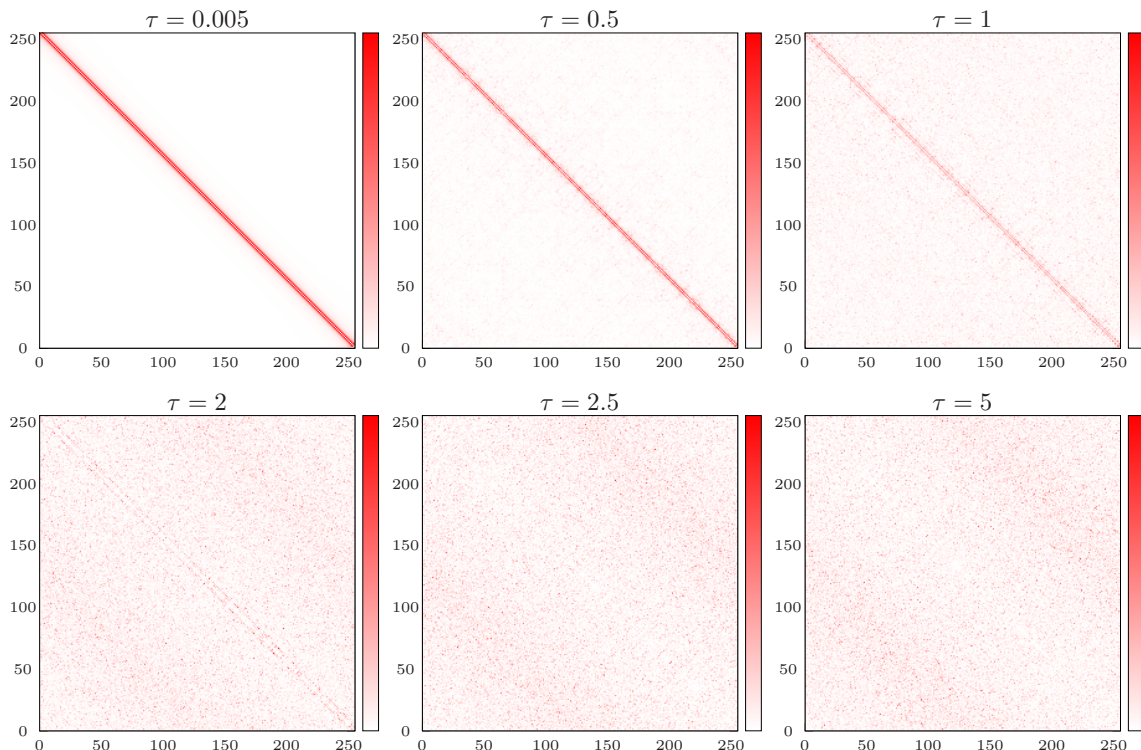


Figure 13. EL matrices corresponding to a chain with $N = 256$ and different values of $\tau = 0.005, 0.5, 1, 2, 2.5$ and 5 , for $t = 1275 T$. The colorbox has always the same range, saturating at an EL intensity of 0.05 .

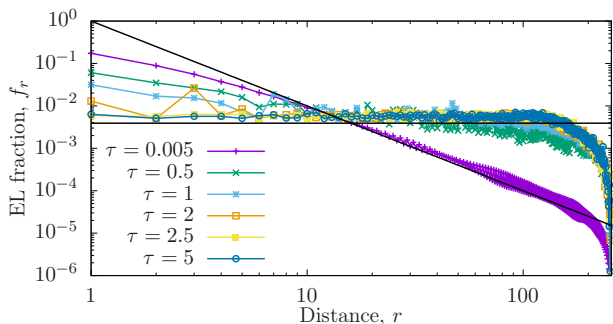


Figure 14. Fraction of the EL along the different subdiagonals for $N = 256$ and $t = 1275 T$, for different values of τ . The straight lines denote the expected power-law behavior for low τ , r^{-2} , and the constant behavior $f_r \sim 1/N$ for large values of τ .

observables roughly coincide with their expected values within the random Slater ensemble. We conjecture that the long-term evolution can be described in both regimes as a generalized random Slater ensemble, in which the expected values of these occupations are forced towards their values on the initial state.

The physical picture can be ascertained by looking at the *entanglement links* (EL), a recently introduced tool which allows us to represent the EE of all possible blocks from a weighted adjacency matrix, to a good approximation. Indeed, the EL matrix allows the geometry asso-

ciated to the entanglement to become manifest. For the fast regime, the EL structure is still one-dimensional, but for the slow phase the EL spread, and the entanglement geometry blurs. The system, effectively, *forgets* that it was 1D.

This work opens up several questions. The full characterization of the fast regime should be performed extending the random Slater ensemble in a suitable way through the use of the conserved quantities. Moreover, integrability plays an important role in our physical system, so it is relevant to consider what happens in its absence. Also, it is interesting to consider a continuous movement of the obstacle, instead of discrete, or to attenuate the effect of the obstacle, making the hopping at the affected link reduced to a certain value, instead of dropping to zero.

Also, we intend to consider different types of motion of the obstacle, other than moving it with a constant speed, and to apply this formalism to the case of the vacuum on a curved background metric, which in many cases just amounts to an inhomogeneous set of hopping parameters [39, 48, 49].

ACKNOWLEDGMENTS

We would like to acknowledge G. Sierra and N. Samos for very useful discussions. This work was funded by the Spanish government through grants PGC2018-094763-

Appendix A: Explicit calculation of Eq. (29)

We rewrite (28) using (18), and we obtain

$$\langle H_2(\mu) \rangle = -\frac{1}{4\pi\mu} \int_{-a}^a \left[\frac{\log\left(\frac{1-\lambda}{2}\right)}{1+\lambda} + \frac{\log\left(\frac{1+\lambda}{2}\right)}{1-\lambda} \right] \sqrt{a^2 - \lambda^2} d\lambda = -\frac{1}{2\pi\mu} \int_{-a}^a \frac{\log\left(\frac{1+\lambda}{2}\right)}{1-\lambda} \sqrt{a^2 - \lambda^2} d\lambda, \quad (\text{A1})$$

where we use the variable $a = 2\sqrt{\mu(1-\mu)}$ for convenience, and we have made the change of variable $\lambda \mapsto -\lambda$ in the first term. Since $0 < \mu < \frac{1}{2}$, we have $0 < a < 1$. To evaluate this integral, we consider the complex valued function

$$f_1(z) = \frac{\log\left(\frac{1+z}{2}\right)}{1-z} (z^2 - a^2)^{1/2}, \quad z \in \mathbb{C},$$

where $0 < a < 1$, the root has a branch cut on $[-a, a]$, and the logarithm has a branch cut on $(-\infty, -1]$.

We fix $R > a$ and we take an indented contour along the real axis, avoiding the branch points $z = \pm a$ and the singularity at $z = -1$ with small circles of radius ε , and winding around the pole at $z = 1$ once in counterclockwise direction with a circular arc C_R of radius R centered at the origin. See Figure 15.

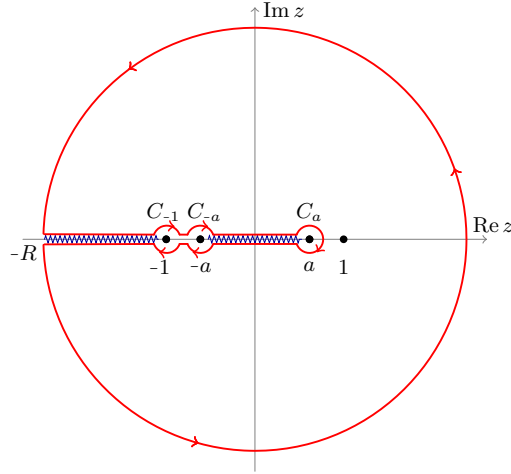


Figure 15. Contour for complex integration.

The boundary values of the function $f_1(z)$ (positive on the left and negative on the right of the contour, with the given orientation) are

$$f_{1\pm}(x) = \begin{cases} -\frac{\log\left(-\frac{1+x}{2}\right) \pm \pi i}{1-x} \sqrt{x^2 - a^2}, & x \in (-\infty, -1 - \varepsilon), \\ -\frac{\log\left(\frac{1+x}{2}\right)}{1-x} \sqrt{x^2 - a^2}, & x \in (-1 + \varepsilon, -a - \varepsilon), \\ \pm i \frac{\log\left(\frac{1+x}{2}\right)}{1-x} \sqrt{a^2 - x^2}, & x \in (-a + \varepsilon, a - \varepsilon). \end{cases}$$

The integrals on the small circles tend to 0 as $\varepsilon \rightarrow 0$, writing $z = \pm a + \varepsilon e^{i\theta}$ or $z = -1 + \varepsilon e^{i\theta}$, and the function $f_1(z)$ has a simple pole at $z = 1$. The residue theorem implies that

$$2i \int_{-a}^a \frac{\log\left(\frac{1+x}{2}\right)}{1-x} \sqrt{a^2 - x^2} dx - 2\pi i \int_{-R}^{-1} \frac{\sqrt{x^2 - a^2}}{1-x} dx + \int_{C_R} f_1(z) dz = 2\pi i \operatorname{res}_{z=1} f_1(z) = 2\pi i \lim_{z \rightarrow 1} (z-1) f_1(z) = 0, \quad (\text{A2})$$

and as a consequence

$$\int_{-a}^a \frac{\log\left(\frac{1+x}{2}\right)}{1-x} \sqrt{a^2-x^2} dx = \pi \int_1^R \frac{\sqrt{x^2-a^2}}{1+x} dx - \frac{1}{2i} \int_{C_R} f_1(z) dz. \quad (\text{A3})$$

In order to evaluate the right hand side, we want to take the limit $R \rightarrow \infty$, but both the integral on $(1, R)$ and the integral on C_R diverge, so we subtract and add the two leading terms:

$$\begin{aligned} \pi \int_1^R \frac{\sqrt{x^2-a^2}}{1+x} dx &= \pi \int_1^R \left[\frac{\sqrt{x^2-a^2}}{1+x} - 1 + \frac{1}{x} \right] dx + \pi \int_1^R \left[1 - \frac{1}{x} \right] dx \\ &= \pi \int_1^R \left[\frac{\sqrt{x^2-a^2}}{1+x} - 1 + \frac{1}{x} \right] dx + \pi R - \pi - \pi \log R, \end{aligned}$$

and now the integral is convergent on $(1, R)$. Similarly,

$$\begin{aligned} -\frac{1}{2i} \int_{C_R} f_1(z) dz &= -\frac{1}{2i} \int_{C_R} \frac{\log\left(\frac{1+z}{2}\right)}{1-z} (z^2-a^2)^{1/2} dz \\ &= -\frac{1}{2i} \int_{C_R} \left[\frac{\log\left(\frac{1+z}{2}\right)}{1-z} (z^2-a^2)^{1/2} + \log z - \log 2 + \frac{\log z - \log 2 + 1}{z} \right] dz \\ &\quad + \frac{1}{2i} \int_{C_R} \left[\log z - \log 2 + \frac{\log z - \log 2 + 1}{z} \right] dz \\ &= -\frac{1}{2i} \int_{C_R} \left[\frac{\log\left(\frac{1+z}{2}\right)}{1-z} (z^2-a^2)^{1/2} + \log z - \log 2 + \frac{\log z - \log 2 + 1}{z} \right] dz \\ &\quad - \pi R + \pi \log R + \pi - \pi \log 2, \end{aligned}$$

writing $z = Re^{i\theta}$, in order to calculate the last integral. Thus, (A3) becomes

$$\begin{aligned} \int_{-a}^a \frac{\log\left(\frac{1+x}{2}\right)}{1-x} \sqrt{a^2-x^2} dx &= \pi \int_1^R \left[\frac{\sqrt{x^2-a^2}}{1+x} - 1 + \frac{1}{x} \right] dx \\ &\quad - \frac{1}{2i} \int_{C_R} \left[\frac{\log\left(\frac{1+z}{2}\right)}{1-z} (z^2-a^2)^{1/2} + \log z - \log 2 + \frac{\log z - \log 2 + 1}{z} \right] dz - \pi \log 2. \quad (\text{A4}) \end{aligned}$$

Now the integrand on C_R is $\mathcal{O}\left(\frac{\log z}{z^2}\right)$ as $z \rightarrow \infty$, so the integral over C_R tends to 0 when $R \rightarrow \infty$. This leads to

$$\int_{-a}^a \frac{\log\left(\frac{1+x}{2}\right)}{1-x} \sqrt{a^2-x^2} dx = \pi \int_1^\infty \left[\frac{\sqrt{x^2-a^2}}{1+x} - 1 + \frac{1}{x} \right] dx - \pi \log 2, \quad (\text{A5})$$

which is a somewhat simpler integral, since a (or μ) does not appear in the limits of integration. We can calculate the indefinite integral

$$J(x) = \int \frac{\sqrt{x^2-a^2}}{1+x} dx \quad (\text{A6})$$

directly: if we make the change of variable $x = a \cosh t$, we have

$$J(t) = a^2 \int \frac{\sinh^2 t}{1+a \cosh t} dt. \quad (\text{A7})$$

Now we write the hyperbolic functions in terms of exponentials, and make the change $v = e^t$:

$$J(v) = \frac{a}{2} \int \frac{v^4 - 2v^2 + 1}{v^2(v^2 + 2v/a + 1)} dv = \frac{a}{2} \int \left(1 - \frac{\frac{2}{a}v^3 + v^2}{v^2(v^2 + 2v/a + 1)} \right) dv. \quad (\text{A8})$$

The roots of the denominator are $v = 0$ and

$$v_{\pm} = \frac{-1 \pm \sqrt{1 - a^2}}{a}.$$

If we do partial fractions, we obtain

$$\frac{\frac{2}{a}v^3 + v^2}{v^2(v^2 + 2v/a + 1)} = \frac{\frac{2}{a}}{v} - \frac{1}{v^2} - \frac{2\sqrt{1 - a^2}}{a(v - v_+)} + \frac{2\sqrt{1 - a^2}}{a(v - v_-)},$$

and therefore

$$J(v) = \frac{av}{2} - \log v - \frac{2}{av} - \sqrt{1 - a^2} \log \left(\frac{v - v_-}{v - v_+} \right) + C.$$

We recall that $x = a \cosh t$, so $2x = ae^t + ae^{-t}$. It follows that $e^t = x \pm \sqrt{x^2 - a^2}$, and we take the plus sign because $x = \infty$ corresponds to $t = \infty$. Therefore, $v = e^t = x + \sqrt{x^2 - a^2}$.

We combine the previous primitive with those corresponding to the terms $-1 + 1/x$ that fix the divergence at infinity, and then

$$\lim_{x \rightarrow \infty} J(v) = \lim_{x \rightarrow \infty} \left[\frac{av}{2} - \log v - \frac{2}{av} - \sqrt{1 - a^2} \log \left(\frac{v - v_-}{v - v_+} \right) - x + \log x \right] = -\log \frac{2}{a}.$$

At $x = 1$, we have $v(1) = 1 + \sqrt{1 - a^2}$, so we obtain

$$J(1) = -1 + \sqrt{1 - a^2} - (1 + \sqrt{1 - a^2}) \log(1 + \sqrt{1 - a^2}) + \log a$$

Therefore, we obtain

$$\begin{aligned} \int_1^{\infty} \left[\frac{\sqrt{x^2 - a^2}}{1 + x} - 1 + \frac{1}{x} \right] dx &= -\log \frac{2}{a} + 1 - \sqrt{1 - a^2} + (1 + \sqrt{1 - a^2}) \log(1 + \sqrt{1 - a^2}) - \log a \\ &= -\log 2 + 1 - (1 - 2\mu) + 2(1 - \mu) \log(2(1 - \mu)) \\ &= \log 2 - 2\mu \log 2 + 2\mu + 2(1 - \mu) \log(1 - \mu), \end{aligned}$$

using that $a = 2\sqrt{\mu(1 - \mu)}$, so $1 - a^2 = (1 - 2\mu)^2$. Replacing this into (A5), we obtain

$$\begin{aligned} \langle H_2(\mu) \rangle &= -\frac{1}{2\mu} \int_1^{\infty} \left[\frac{\sqrt{x^2 - a^2}}{1 + x} - 1 + \frac{1}{x} \right] dx + \frac{\log 2}{2\mu} = -\frac{1}{2\mu} [\log 2 - 2\mu \log 2 + 2\mu + 2(1 - \mu) \log(1 - \mu)] + \frac{\log 2}{2\mu} \\ &= \log 2 - 1 - \frac{1 - \mu}{\mu} \log(1 - \mu), \end{aligned} \quad (\text{A9})$$

which proves the result.

-
- [1] H.B.G. Casimir, *On the attraction between two perfectly conducting plates*, *Indag. Math.* **10**, 261 (1948).
[2] G.T. Moore, *Quantum Theory of the Electromagnetic Field in a Variable-Length One-Dimensional Cavity*, *J. Math. Phys.* **11**, 2679 (1970).

- [3] D.T. Alves, C. Farina, P.A. Maia Neto, *Dynamical casimir effect with Dirichlet and Neumann boundary conditions*, *J. Phys. A: Math. Gen.* **36**, 11333 (2003).
[4] M. Srednicki, *Entropy and area*, *Phys. Rev. Lett.* **71**, 666 (1993).

- [5] J. Eisert, M. Cramer, M.B. Plenio, *Area laws for the entanglement entropy - a review*, Rev. Mod. Phys. **82**, 277 (2010).
- [6] M.B Hastings, *An area law for one-dimensional quantum systems*, JSTAT P08024 (2007).
- [7] P. Calabrese, J.L. Cardy, *Entanglement entropy and quantum field theory*, JSTAT P06002 (2004).
- [8] P. Calabrese, J. Cardy, *Entanglement entropy and conformal field theory*, J. Phys. A **42**, 504005 (2009).
- [9] S. Singha Roy, S.N. Santalla, J. Rodríguez-Laguna, G. Sierra, *Entanglement as geometry and flow*, Phys. Rev. B **101**, 195134 (2020).
- [10] S. Singha Roy, S.N. Santalla, G. Sierra, J. Rodríguez-Laguna, *Link representation of the entanglement entropies for all bipartitions*, J. Phys. A: Math. Theor. **54**, 305301 (2021).
- [11] S.N. Santalla, S. Singha Roy, G. Sierra, J. Rodríguez-Laguna, *Entanglement links and the quasi-particle picture*, Phys. Rev. B **107**, 121114 (2023).
- [12] D. Stefanatos, *Optimal shortcuts to adiabaticity for a quantum piston*, Automatica **49**, 3079 (2013).
- [13] D. Jaksch, P. Zoller, *The cold atom Hubbard toolbox*, Ann. Phys. **315**, 52 (2005).
- [14] M. Lewenstein, A. Sanpera, V. Ahufinger, *Ultracold atoms in optical lattices*, Oxford University Press (2012).
- [15] C. Gross, I. Bloch, *Quantum simulations with ultracold atoms in optical lattices*, Science **357**, 995 (2017).
- [16] I. Peschel, *Entanglement in solvable many-particle models*, Braz. J. Phys. **42**, 267 (2012).
- [17] N. Goldman, J. Dalibard, *Periodically driven quantum systems: effective Hamiltonians and engineered gauge fields*, Phys. Rev. X **4**, 031027 (2014).
- [18] M. Bukov, M. Heyl, D.A. Huse, A. Polkovnikov, *Heating and many-body resonances in a periodically driven two-band system*, Phys. Rev. B **93**, 155132 (2016).
- [19] K. Seetharam, P. Titum, M. Kolodrubetz, G. Refael, *Absence of thermalization in finite isolated interacting Floquet systems*, Phys. Rev. B **97**, 014311 (2018).
- [20] A. Eckardt, *Colloquium: Atomic quantum gases in periodically driven optical lattices*, Rev. Mod. Phys. **89**, 011004 (2017).
- [21] L. D'Alessio, M. Rigol, *Long-time behavior of isolated periodically driven interacting lattice systems*, Phys. Rev. X **4**, 041048 (2014).
- [22] A. Lazarides, A. Das, R. Moessner, *Equilibrium states of generic quantum systems subject to periodic driving*, Phys. Rev. E **90**, 012110 (2014).
- [23] P. Ponte, A. Chandran, Z. Papić, D.A. Abanin, *Periodically driven ergodic and many-body localized quantum systems*, Ann. Phys. **353**, 196 (2015).
- [24] R. Moessner, S.L. Sondhi, *Equilibration and order in quantum Floquet matter*, Nat. Phys. **13**, 424 (2017).
- [25] N. Tsuji, *Floquet states*, arXiv:2301.12676 (2023).
- [26] M.V. Berry, M. Tabor, *Level clustering in the regular spectrum*, Proc. R. Soc. Lond. A **356**, 375 (1977).
- [27] O. Bohigas, M. J. Giannoni, C. Schmit, *Characterization of chaotic quantum spectra and universality of level fluctuation laws*, Phys. Rev. Lett. **52**, 1 (1984).
- [28] M.L. Mehta, *Random matrices*, Elsevier (2004).
- [29] J.A. Scaramazza, B. Sriram Shastry, E.A. Yuzbashyan, *Integrable matrix theory: level statistics*, Phys. Rev. E **94**, 032106 (2016).
- [30] D.N. Page, *Average entropy of a subsystem*, Phys. Rev. Lett. **71**, 1291 (1993).
- [31] E. Bianchi, L. Hackl, M. Kieburg, M. Rigol, L. Vidmar, *Volume-law entanglement entropy of typical pure quantum states*, PRX Quantum **3**, 030201 (2022).
- [32] J. Magán, *Random free fermions: an analytical example of eigenstate thermalization*, Phys. Rev. Lett. **116**, 030401 (2016).
- [33] E. Bianchi, L. Hackl, M. Kieburg, *The page curve for fermionic gaussian states*, Phys. Rev. B, **103**, 241118 (2021).
- [34] Y. Huang, L. Wei, *Entropy fluctuation formulas of fermionic Gaussian states*, arXiv:2211.16709 (2022).
- [35] K. Życzkowski, H.-J. Sommers, *Truncations of random unitary matrices*, J. Phys. A: Math. Gen. **33**, 2045 (2000).
- [36] B. Collins, *Product of random projections, Jacobi ensembles and universality properties arising from free probability*, Prob. Theor. Rel. Fields **133**, 315 (2005).
- [37] B. Mula, N. Samos Sáenz de Buruaga, G. Sierra, S.N. Santalla, J. Rodríguez-Laguna, *Depletion in fermionic chains with inhomogeneous hoppings*, Phys. Rev. B **106**, 224204 (2022).
- [38] E.H. Lieb, D.W. Robinson, *The finite group velocity of quantum spin systems*, Comm. Math. Phys., **28**, 251 (1972).
- [39] B. Mula, S.N. Santalla, J. Rodríguez-Laguna, *Casimir forces on deformed fermionic chains*, Phys. Rev. Research **3**, 013062 (2021).
- [40] A. Chenu, J. Molina-Vilaplana, A. del Campo, *Work statistics, Loschmidt echo and information scrambling in chaotic quantum systems*, Quantum **3**, 127 (2019).
- [41] H.J.D. Miller, M. Scandi, J. Anders, M. Perarnau-Llobet, *Work Fluctuations in Slow Processes: Quantum Signatures and Optimal Control*, Phys. Rev. Lett. **123**, 230603 (2019).
- [42] M. Scandi, H.J.D. Miller, J. Anders, M. Perarnau-Llobet, *Quantum work statistics close to equilibrium*, Phys. Rev. Res. **2**, 023377 (2020).
- [43] H.J.D. Miller, M. H. Mohammady, M. Perarnau-Llobet, G. Guarneri, *Thermodynamic Uncertainty Relation in Slowly Driven Quantum Heat Engines*, Phys. Rev. Lett. **126**, 210603 (2021).
- [44] K. Zawadzki, A. Kiely, G.T. Landi, S. Campbell, *Non-Gaussian work statistics at finite-time driving*, Phys. Rev. A **107**, 012209 (2023).
- [45] Y. Y. Atas, E. Bogomolny, O. Giraud, and G. Roux. *Distribution of the ratio of consecutive level spacings in random matrix ensembles*. Phys. Rev. Lett., 110:084101, Feb 2013.
- [46] N.D. Chavda, H.N. Deota, V.K.B. Kota, *Poisson to GOE transition in the distribution of the ratio of consecutive level spacings*, Phys. Lett. A **378**, 3012 (2014).
- [47] M. Fagotti, P. Calabrese, J.E. Moore, *Entanglement spectrum of random-singlet quantum critical points*, Phys. Rev. B **83**, 045110 (2011).
- [48] O. Boada, A. Celi, J.I. Latorre, M. Lewenstein, *Dirac equation for cold atoms in artificial curved spacetimes*, New J. Phys. **13**, 035002 (2011).
- [49] J. Rodríguez-Laguna, J. Dubail, G. Ramírez, P. Calabrese, G. Sierra, *More on the rainbow chain: entanglement, space-time geometry and thermal states*, J. Phys. A **50**, 164001 (2017).